FEBS Letters 585 (2011) 3593–3599

journal homepage: www.FEBSLetters.org

Crystal structure of the EphA4 protein tyrosine kinase domain in the apo- and dasatinib-bound state

Carine Farenc [a], Patrick H.N. Celie [b], Cornelis P. Tensen [c], Iwan J.P. de Esch [d], Gregg Siegal [a,*]

[a] Protein Chemistry Group, Leiden Institute of Chemistry, Leiden University, Leiden, The Netherlands
[b] Division of Biochemistry, The Netherlands Cancer Institute, Amsterdam, The Netherlands
[c] Department of Dermatology, Leiden University Medical Center, Leiden, The Netherlands
[d] Leiden/Amsterdam Center for Drug Research (LACDR), Division of Medicinal Chemistry, Faculty of Sciences, VU University Amsterdam, Amsterdam, The Netherlands

ARTICLE INFO

Article history:
Received 29 August 2011
Revised 12 October 2011
Accepted 13 October 2011
Available online 22 October 2011

Edited by Kaspar Locher

Keywords:
Receptor tyrosine kinase
EphA4
Dasatinib
X-ray crystallography
Three-dimensional structure

ABSTRACT

The Eph family of receptor tyrosine kinases regulates diverse cellular processes while the overexpression of a member of this family, EphA4, has been reported in a variety of malignant carcinomas. To gain insight into molecular mechanisms and to facilitate structure-based inhibitor design, we solved the crystal structure of the native EphA4 kinase domain in both the apo and dasatinib bound forms. Analysis of the two structures provides insight into structural features of inhibitor binding and revealed a hydrophobic back-pocket in the ATP- binding site of EphA4 which was previously unidentified. The structures suggest a route towards development of novel and specific inhibitors.

1. Introduction

The erythropoietin-producing hepatocellular (Eph) family of receptor tyrosine kinases are key regulators of diverse cellular functions including cell proliferation, differentiation and migration [1]. In addition to the roles that kinases are traditionally associated with such as mitogenesis, Eph receptors are also key factors in processes such as axon growth and angiogenesis [2,3]. To date fourteen different human Eph receptors and eight different ligands, known as ephrins, have been identified [4]. The ephrins are divided into two subclasses A and B, based on their GPI-anchored or transmembrane structure, respectively. The receptors are also classified into two families, EphA and EphB, depending on the binding affinity for either the A or B ephrins, respectively [5]. The most well known exception to this general rule is EphA4, which binds both A- and B-class ligands [6–8].

In addition to its normal role in cellular regulation, over expression of EphA4 has been observed in a variety of malignant carcinomas including gastric cancer [9], prostate cancer [10] and cutaneous lymphomas [11] among others. Furthermore, the overexpression of EphA4 seems to be critical for tumor growth in a significant percentage of prostate cancers [10]. In addition to its potential role in oncology, data obtained from EphA4-knockout mice suggest that blocking EphA4 function might be beneficial for the treatment of spinal cord injuries [12]. The ability to modulate the activity of this family of receptors could prove useful and therefore they represent interesting therapeutic targets.

Eph receptors share a common topology where the extracellular region consists of: an N-terminal ephrin binding domain, a cysteine-rich region and two fibronectin type III repeats near the single membrane-spanning segment. The cytoplasmic region contains a short amino acid sequence referred to as the juxtamembrane segment (JMS), the highly conserved tyrosine kinase domain (KD), a C terminal sterile α domain (SAM) and a PDZ domain binding motif [13]. The JMS domain contains tyrosine residues that must be phosphorylated to allow full activation of the kinase activity [14] which is unique to the Eph receptors. In the crystal structure of EphB2, the JMS forms an α-helix that interacts with the kinase domain and prevents it from adopting an ordered, active structure, thus providing another level of regulation [15]. NMR studies of EphB2 have shown that upon activating phosphorylation events, the JMS and KD undergo increased conformational exchange [16]. It was postulated that autoinhibition was achieved via the JMS

Abbreviations: KD, kinase domain; JMS, juxtamembrane segment; RTKs, receptor tyrosine kinases

* Corresponding author. Fax: +31 71 527 4603.
E-mail address: g.siegal@chem.leidenuniv.nl (G. Siegal).

0014-5793/$36.00
doi:10.1016/j.febslet.2011.10.028

"locking" the N and C terminal lobes of the KD in an unproductive conformation. Thus the additional regulatory switch represented by the JMS could potentially also be a target for inhibitor design.

Dasatinib is a well known kinase inhibitor that was approved for use in cases of imatinib resistance in chronic myeloid leukemia (CML) [17]. Although dasatinib was primarily designed as a selective inhibitor of the Src and BCR-Abl kinases [18], it was found to have a broader inhibition spectrum which includes members of the Eph family [19,20]. However, no crystal structure of dasatinib in complex with a member of this family has thus far been elucidated. Since no structure of the wild type kinase domain was available, we wished to gain insight into the active form and to facilitate structure-based inhibitor design by determining the crystal structure of the EphA4 kinase domain in both the apo and dasatinib bound forms.

2. Materials and methods

2.1. Plasmid construction

The murine EphA4 kinase domain (amino acids 606–846) was commercially synthesized with codon usage optimized for expression in *Escherichia coli*. The gene was cloned into a pET28a vector (Invitrogen) generating an N-terminal 6His tag fused to the kinase domain with an intervening region containing an amino acid sequence efficiently hydrolyzed by the tobacco etch virus (TEV) protease. The purified protein contained a single non-coded glycine at the N terminus after cleavage.

2.2. Expression and purification of EphA4 kinase domain

The details of expression and purification of the EphA4 kinase domain can be found in Supplementary material.

2.3. Crystallization of the EphA4 kinase domain

Crystals were grown at 20 °C using the sitting-drop vapor-diffusion method. The purified EphA4 kinase domain was mixed with an equal volume of a reservoir solution containing 15–21% polyethylene glycol 10 K, 100 mM ammonium acetate and 100 mM bis–tris pH 5.5. Rod-like crystals appeared after 1–3 days.

2.4. Co-crystallization of EphA4 kinase domain in complex with dasatinib

Dasatinib (*N*-(2-chloro-6-methylphenyl)-2-(6-(4-(2-hydroxyethyl)piperazin-1-yl)-2-methylpyrimidin-4-ylamino)thiazole-5-carboxamide) [21] was added to the purified protein at a final concentration of 1 mM in dimethyl sulfoxide (molar ratio dasatinib/protein of 3) and mixed with an equal volume of a reservoir solution containing 15–21% polyethylene glycol 10 K, 100 mM ammonium acetate and 100 mM bis–tris pH 5.5. Crystals appeared after 1–3 days.

2.5. X-ray data collection, structure determination and refinement

Crystals were flash frozen using the reservoir solution supplemented with 20% glycerol as a cryoprotectant. Diffraction data for the apo protein was collected at the Swiss Light Source (SLS, beamline X06SA) and at the European Synchrotron Radiation Facilities (ESRF, beamline ID23-2) for the inhibitor bound. Datasets at 1.5 Å for the apo-protein and 1.55 Å for the inhibitor complex were processed using XDS [22] and POINTLESS [23] from the CCP4i suite [24]. The apo-structure was solved by molecular replacement using the program AMoRe [25]. A mutant of EphA4 was used as a search model (PDB ID: 2HEL). From the AMoRe solution, a model was built and input into ARP/wARP [26] for automated tracing. The dasatinib-bound structure was solved by molecular replacement (AMoRe) using the native protein as a search model. The structures were refined using rigid body refinement within the program REFMAC5 [27]. This was followed by restrained refinement with PHENIX [28] interspersed with rounds of model building with COOT [29]. A summary of the data collection and refinements statistics is presented in Supplementary Table S1.

3. Results and discussion

3.1. Apo enzyme structure

The phosphorylated kinase domain of murine EphA4 (residues 606–846, referred to as EphA4 KD) was crystallized in the apo form and the structure was determined at 1.7 Å resolution. The crystallographic model contains one molecule in the asymmetric unit and was refined to an R_{work} = 17.49% and R_{free} = 20.32%. The overall bilobed structure typical of kinases is well ordered except for three N-terminal residues and five C-terminal residues and residues 765–787 of the activation segment. The N-terminal lobe consists of the characteristic five-stranded β sheet and a single large α helix (αC) while the C-terminal lobe is larger and mainly α-helical, but includes a two stranded anti-parallel β-sheet as expected (Fig. 1). Protein kinases contain a number of conserved elements that contribute to the enzyme activity including: a hinge region connecting the two lobes, a glycine rich loop or p-loop, a catalytic loop and an activation loop, all of which are present in the EphA4 structures. The activation loop includes a consensus Asp–Phe–Gly (DFG) motif sequence that is critical for ATP binding [30] and is highly conserved among kinases [31].

The present structure is characteristic of a phosphorylated, and therefore activated, form of a kinase domain [32]. First, the αC-helix is in the ATP proximal position allowing the formation of the conserved Lys^{653}–Glu^{670} salt bridge which coordinates the alpha and beta phosphate groups of ATP *via* polar contacts. Second, the activation loop is disorganized and adopts the so-called "DFG-in" conformation [33] with the side-chain of Phe^{765} pointing towards the interior of the molecule (Fig. 1B).

3.2. Comparison of Eph receptor crystal structures

An EphA4 protein consisting of the kinase domain and the adjacent juxtamembrane segment (JMS), which comprises the mutations Y596/602F in the JMS and Y742A in the KD, has been previously crystallized (PDB ID: 2HEL) [16]. We refer to this structure as EphA4 JMS–KD. Although the resolution of this structure is 2.35 Å, the JMS is almost completely disordered. Overall, the structures of the two proteins are very similar with an r.m.s. deviation of 0.633 Å for the superimposition of 208 Cα atoms (Fig. 2A and Supplementary Table S2). The C terminal lobe is nearly identical in the two structures with the exception that five less amino acid residues of the activation loop of EphA4 KD could be modeled. As the catalytic and activation loops are spatially close to each other in the EphA4 KD structure, the presence of the bulky side-chain of Tyr^{742} in the catalytic loop leads to reduced interaction with the activation loop and its subsequent disorganization. The Y742A mutation in EphA4 JMS–KD removes the tyrosine side-chain allowing repacking and stabilization of the activation loop. In contrast, the N-terminal lobe shows greater differences between the KD and JMS–KD structures. The largest difference observed is in the location of the αC-helix where a 4.5 Å movement of the Cα of Asp^{661} upward and outward in the KD structure causes the displacement of the entire alpha helix. The αC-helix contains a kink that leads to a bend of the long axis by 14° at about the midpoint

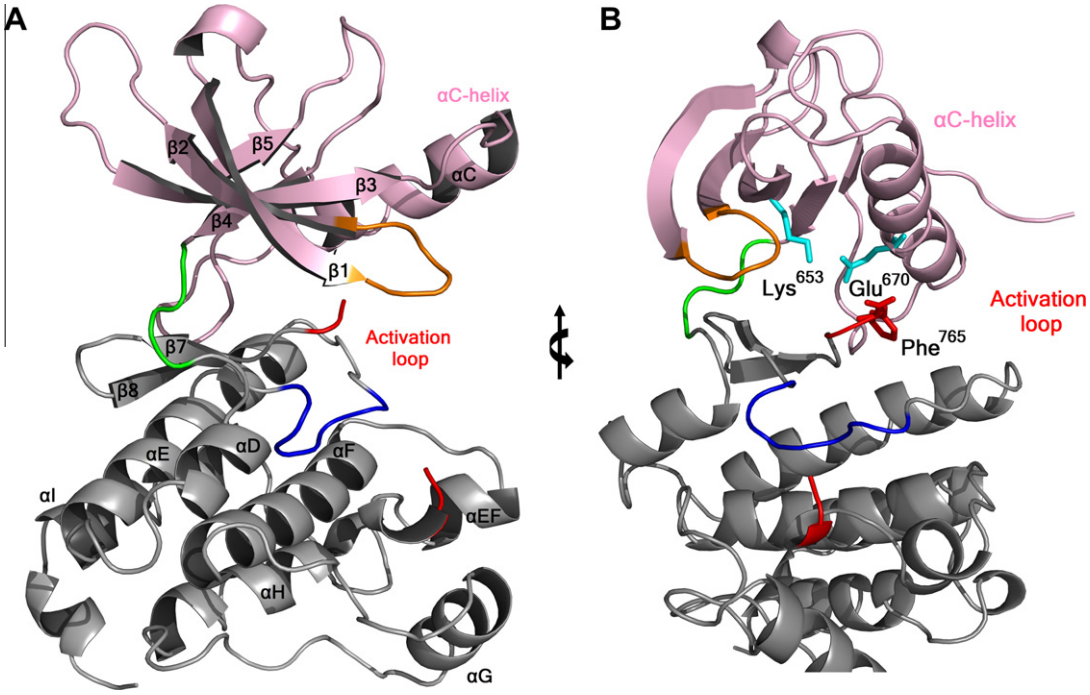

Fig. 1. Overview of the crystal structure of the EphA4 kinase domain. (A) Ribbon representation of the apo-EphA4 kinase domain crystal structure. The N-terminal lobe, shown in pink, consists of a five-stranded anti-parallel β-sheet and one α-helix (αC). The C-terminal lobe, in grey, is mainly α-helical. The p-loop is colored orange, the hinge region in green, the catalytic loop in blue and the activation loop in red. (B) Same as in A with a 90° rotation about the z axis. Residues important for kinase activation (Lys^{653}, Glu^{670} and Phe^{765}) are shown in stick representation. All molecular graphics were generated with PyMOL (The PyMOL Molecular Graphics System; DeLano Scientific, 2002).

of the helix (Fig. 2A). The kink is similar in both structures, however, the relative position of the alpha helix is different, which in turn influences the position of the conserved Lys–Glu salt bridge. The salt bridge is also influenced by the position of the p-loop which is shifted upwards in the KD structure compared to the JMS–KD structure. Thus, although the two crystals structures share an almost identical amino acid sequence, there are significant structural differences.

To try and determine whether the structural differences between EphA4 KD and JMS–KD are related to the presence of the JMS, we compared this pair to the structures of another KD JMS–KD pair from the Eph family. Crystal structures of the closely related kinase EphB2 have been solved both in the active state (EphB2 KD, PDB ID: 2HEN) which comprise a D754A mutation in the activation loop [16]) and the auto-inhibited state (EphB2 JMS–KD, PDB ID: 1JPA) [15]. In the EphB2 JMS–KD structure, a Y604/610A mutation in the JMS has been made to prevent activation, which results in an enzyme with constitutively low activity [14]. Overall, the structures of the two pairs of kinases are similar except for the αC-helix and the p-loop which present slight changes (Fig. 2B and Supplementary Table S2). The αC-helix exhibits a similar kink in all the structures, the cause of which was previously attributed to the JMS [15]. However, a subsequent crystal structure of EphA2 was reported which also exhibited a bent conformation of the αC-helix despite the absence of a JMS (Fig. 2C) [34]. The situation is similar with the present crystal structure of EphA4 KD, i.e., a kink in the αC-helix even though the JMS is absent. This observation confirms the previous suggestion [16] that the presence of the JMS in the EphA4 JMS–KD structure is not responsible for the kink in the αC-helix. However, the relative position of the αC-helix is different in all the structures (Fig. 2C). In the present structure of active EphA4, the position of the αC-helix is closer to the auto-inhibited JMS–KD of EphB2, indicating that the details of the position of the αC-helix do not necessarily correlate with the state of activity of the kinase.

The variability of the p-loop in all four structures shown in Fig. 2C, which influences the position of the conserved Lys–Glu salt bridge, is even greater than the αC-helix. In the kinase domain of EphA4, the position of the salt bridge is shifted, creating a larger hydrophobic pocket than in the other Eph receptor kinases, including specifically the EphA4 JMS–KD (Fig. 2D). Other Eph receptor kinase domains that have been crystallized without the JMS or mutations lack this hydrophobic pocket due to the position of the salt bridge (Supplementary Fig. S1). In addition, it seems likely that this pocket is present in the active, full-length kinase considering inhibition of EphA4 by dasatinib has been demonstrated in the cell [19] and dasatinib occupies this back pocket in our crystal structure (see below). This newly discovered back-pocket should allow for both enhanced specificity and potency for EphA4 inhibitors.

3.3. Structure of EphA4-dasatinib complex

Dasatinib is an ATP competitive inhibitor that targets multiple kinases. Amongst the numerous targets of dasatinib, it has been shown to inhibit EphA4 [19,20]. Using a commercially available kinase assay (ADP Hunter Plus, DiscoveRx), the IC_{50} of dasatinib for the kinase domain of EphA4 was 25 nM (data not shown). However, no structural information regarding the binding of dasatinib to EphA4 is available. In order to address this issue, dasatinib was co-crystallized with EphA4 KD under conditions identical to the apo protein. The structure of the complex was solved to 1.55 Å resolution and refined to an R_{work} = 18.01% and R_{free} = 20.05% (Fig. 3 and Supplementary Table S1). Structural alignment of the apo and the dasatinib bound forms of EphA4 KD gives an r.m.s deviation of 0.150 Å over 220 Cα atoms. Although the 3D structures are very similar, the B factors of the apo and inhibitor bound proteins are subtly different (Fig. 4). B-factors are a measure of the order in the unit cell. Careful inspection reveals that the backbone atoms have on average slightly lower B-factors in the inhibitor bound complex while the side-chains have somewhat larger B-factors. Dynamic behavior in

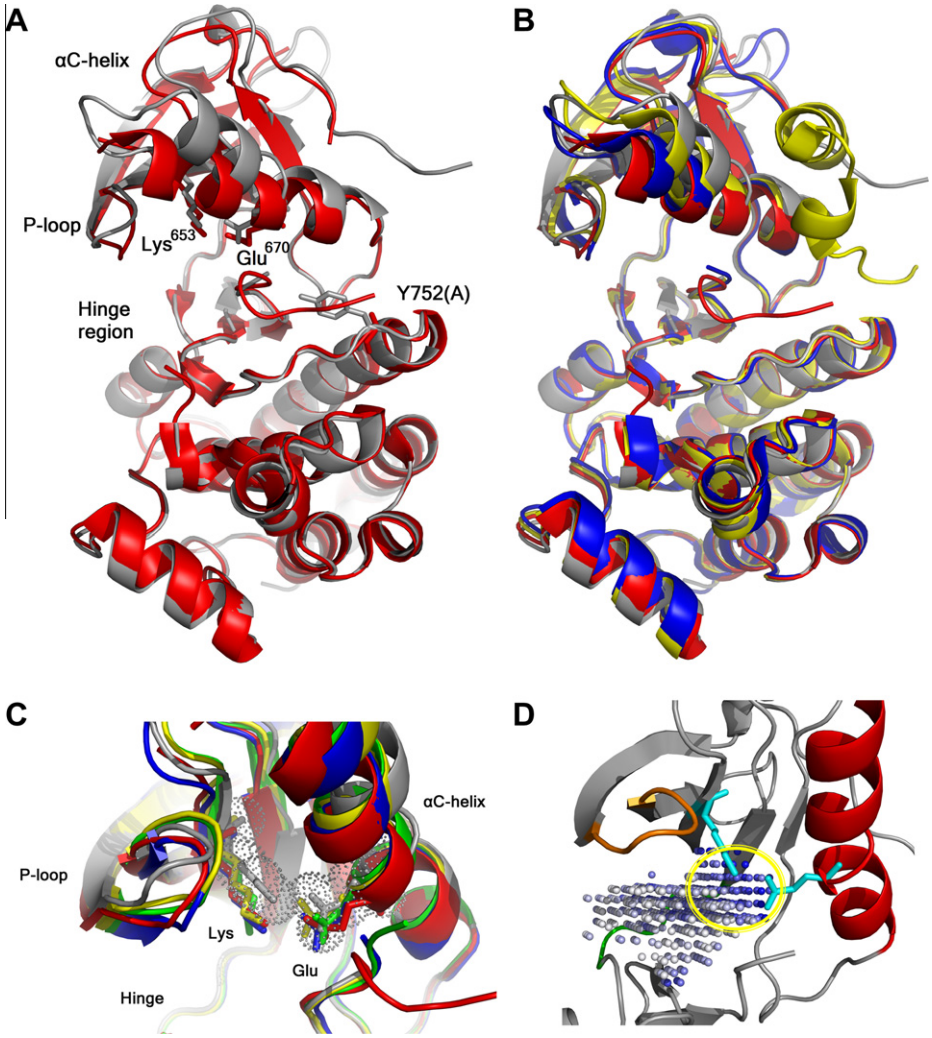

Fig. 2. Comparison of the EphA4 crystal structure with the kinase domain of other Eph receptor. (A) Superimposition of EphA4 structures: EphA4 KD (grey), EphA4 JMS–KD (2HEL, red); Shown in bond representation: the residues contributing to the conserved salt bridge Lys–Glu and the Tyr/Ala residue in the activation loop (B) Superimposition of EphA4 and EphB2 structures: EphA4 KD (grey), EphA4 JMS–KD (2HEL, red), EphB2 KD (2HEN, blue), EphB2 JMS–KD (1JPA, yellow). (C) Superimposition of EphA4, EphB2 and EphA2: closer view of the N-lobe, the residues contributing to the conserved salt bridge Lys–Glu are shown in bond representation while the dots represent the van der Waal's surface of the salt bridge. EphA4 KD (grey), EphA4 JMS–KD (2HEL, red), EphB2 KD (2HEN, blue), EphB2 JMS–KD (1JPA, yellow), EphA2 KD (1MQB, green). (D) Close up view of the ATP binding pocket of EphA4. The dots show the ATP binding pocket and the back hydrophobic pocket is circled in yellow. The orange, green, cyan and red elements represent respectively the p-loop, hinge region, the salt bridge Lys^{653}–Glu^{670} and the αC helix.

solution may give rise to increased B-factors. Interestingly, a similar pattern of dynamic changes on ligand binding (decreased dynamic behavior of the backbone and increased dynamics of the side-chains) has been observed in NMR [35]. The pattern of changes in the B-factors suggests a thermodynamic explanation for binding, i.e., that reduced entropy of the backbone in the dasatinib bound form is compensated by increased entropy in the side-chains. As a result, the net entropic change of ligand binding is minimal. The reduced B-factors for backbone atoms extends slightly further towards the N-terminus in the dasatinib bound protein allowing two additional amino acids to be modeled. As with the apo protein, the αC-helix is in the ATP proximal position allowing the formation of the conserved Lys^{653}–Glu^{670} salt bridge indicative of the kinase active state [32] while the activation loop is also in the "DFG-in" conformation [33].

Dasatinib makes several hydrogen bonds to the hinge and occupies the hydrophobic pocket behind the Thr^{699} residue which is commonly referred to as the 'gatekeeper' residue [36]. The side-chain of the gatekeeper residue sterically controls inhibitor binding to the hydrophobic pocket [37]. There are three main hydrogen bonds between dasatinib and the kinase: one between the nitrogen of the amino-thiazole ring and the amide nitrogen of Met^{702}, another between the amino group of the amino-thiazole ring with the carbonyl oxygen of Met^{702} and a third one between the amide nitrogen of dasatinib and the side-chain hydroxyl oxygen of Thr^{699}. The 2-chloro-6-methyl phenyl group of dasatinib occupies the hydrophobic pocket and makes extensive van der Waal's (vdW) contacts with Lys^{653}, Glu^{670}, Met^{674}, Ile^{683}, Ile^{697} and Thr^{699}. The amino-thiazole ring has vdW's contacts with Leu^{753} and Ala^{651}, in addition to the previously described hydrogen bond. The pyrimidine ring extends out of the binding pocket and makes vdW contact with Ile^{627}. The hydroxyethyl-piperazine group is largely solvent exposed.

In an analysis of the Eph receptor family [20], it was observed that, except for EphA6 and EphA7, dasatinib inhibited all of the Eph receptors. Interestingly, the gatekeeper residue in EphA6 is Val and Ile in EphA7, while in all other members of the family it is Thr. The bulky gatekeeper residues in EphA6 and EphA7 likely obstruct access to the hydrophobic pocket. The pattern of inhibition is not surprising since dasatinib was designed to access the hydrophobic pocket created by the mutation of the gatekeeper residue from Ile to Thr in Abl kinase that lead to resistance to imatinib [17,18]. It seems likely that the mode of binding of

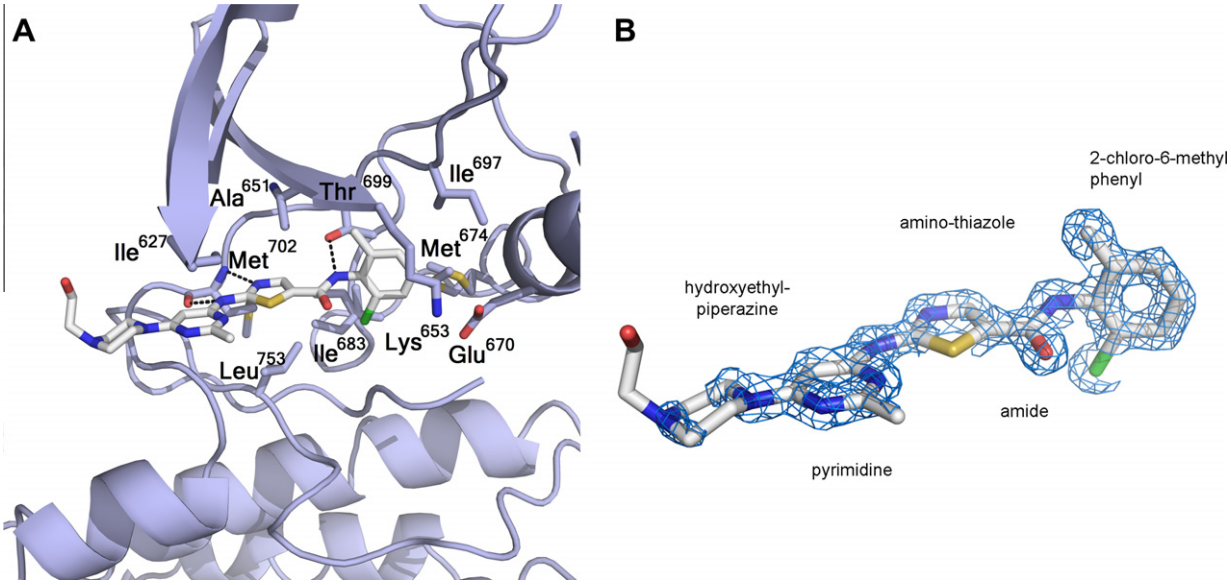

Fig. 3. Binding mode of dasatinib to EphA4. (A) Overview of the binding interaction. Dasatinib and residues that interact with it are shown in bond view, hydrogen bounds are indicated by black dashed lines. (B) View of dasatinib overlaid with the simulated annealing omit-map F_0–F_c electron density contoured at 2σ.

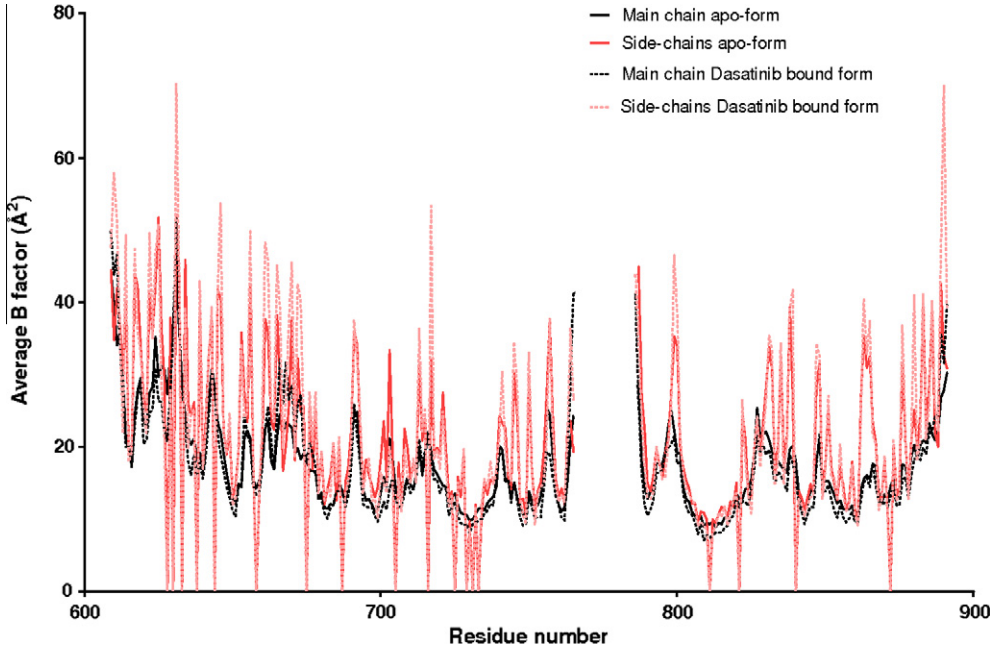

Fig. 4. Average B factor per residue number. In black the values for main chain, and in red values for the side-chains. Solid lines are values for the apo-form and the dashed lines are values for the dasatinib bound form.

dasatinib observed here is similar for the other Eph receptors that are inhibited by this compound.

3.4. Structural comparison with other kinases bound to dasatinib

Since a number of other dasatinib bound structures have been elucidated, it is useful to compare the present structure to these. We have selected four representative structures, two from the Src family (Src [38], and Lyn [39]), the Ableson kinase (Abl [40]) and Bruton's tyrosine kinase (BTK) [41]) for comparison with our dasatinib-bound EphA4 structure. In all five structures, the 2-chloro-6-methyl phenyl group of dasatinib occupies a hydrophobic pocket adjacent to the ATP-binding site behind the gatekeeper residue, which in all cases is a Thr (Fig. 5A). All 5 structures exhibit an αC-helix in the ATP-proximal position, the salt bridge between Lys and Glu and an activation loop with the "DFG-in" conformation. The kink in the αC-helix is present in all the structures and the position of the helix is slightly different in each (Fig. 5B). However, the salt bridge is in the same position in all the structures. Although the binding mode of dasatinib is globally similar in all the structures, two different binding orientations are observed for the 2-chloro-6-methyl phenyl group of dasatinib. The chloride is pointing toward the C-terminal lobe in the Src, Lyn and EphA4 complexes (Fig. 5C), while the chloro substituent is pointing in the opposite direction in the Abl and BTK complexes (Fig. 5D). However, it is not clear why the different binding orientations are observed, it may be related to the resolution. In the present, relatively high resolution EphA4 structure, the orientation of the

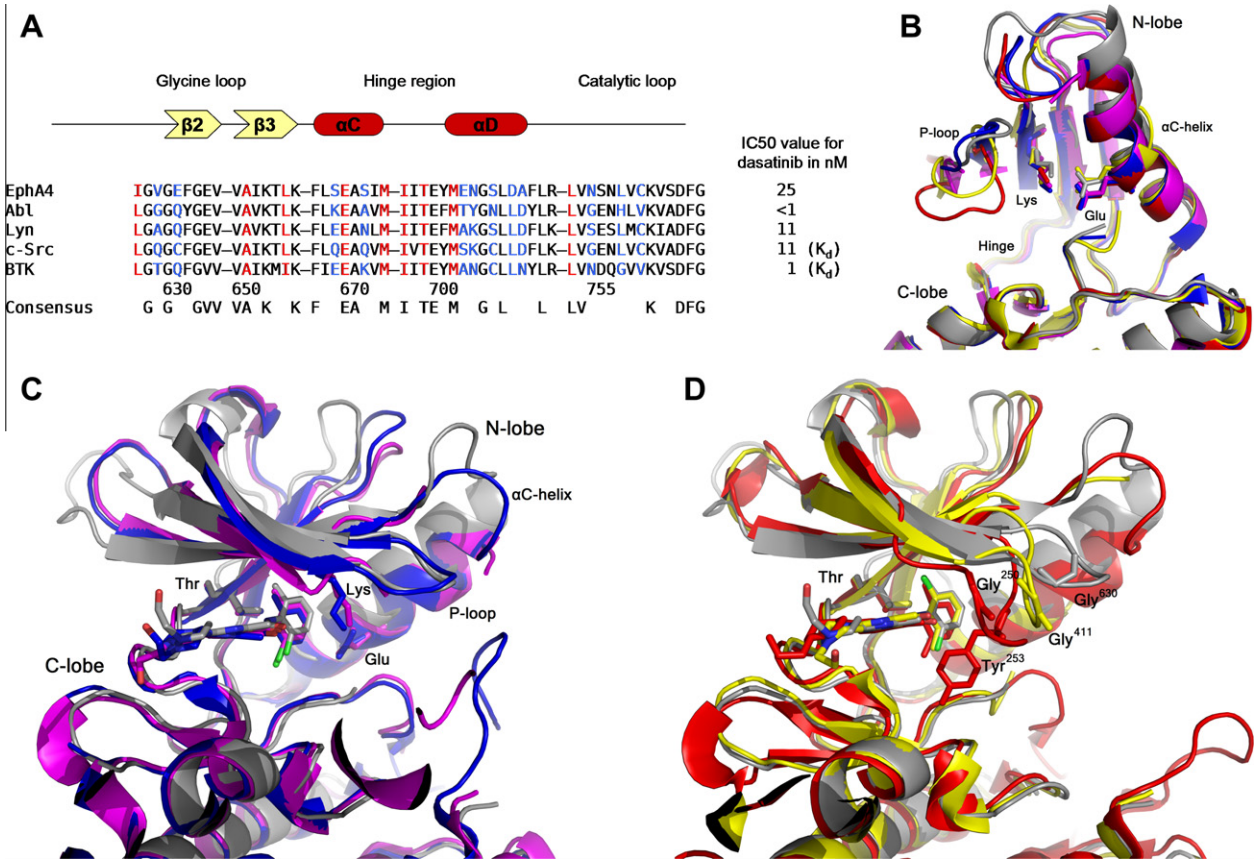

Fig. 5. (A) Sequence alignment of a portion of the EphA4 kinase domain with other RTKs that bind dasatinib: Lyn, BTR, c-Src and Abl. Variable residues are indicated in blue; and the residues that interact with dasatinib are shown in red. The potency of dasatinib inhibition of each kinase is indicated on the right. (B) Superimposition of EphA4 (2Y6O, grey), Lyn (2ZVA, blue), c-Src (3G5D, magenta), BTK (3K54, yellow) and Abl (2GQG, red). The residues contributing to the conserved salt bridge are shown in bond representation. (C) Superimposition of EphA4 (2Y6O, grey), Lyn (2ZVA, blue) and c-Src (3G5D, magenta). The residues contributing to the conserved salt bridge and the gatekeeper residue (Thr) are shown in bond representation. (D) Superimposition of EphA4 (2Y6O, grey), BTK (3K54, yellow) and Abl (2GQG, red), in addition to the residues contributing to the salt bridge and the gatekeeper residue (Thr), selected residues in the p-loop are shown in bond representation (Gly^{250} and Tyr^{253} for Abl, Gly^{411} for BTK and Gly^{630} for EphA4).

chloro substituent pointing toward the C-terminal lobe fit the electron density better.

In addition to the hydrophobic pocket, differences are observed in the p-loop in both Abl and BTK structures compared to EphA4. There is a 7.7 Å movement of the Cα of Abl Gly^{250} towards the ATP binding site in comparison to the corresponding EphA4 Gly^{630} (Fig. 5D). The p-loop of BTK shows a similar movement to Abl, although to a slightly lesser extent, with a 3.65 Å movement of the Cα of BTK Gly^{411} towards the ATP binding site in comparison to the corresponding Gly^{630} of EphA4. Moreover, Abl Tyr^{253} makes several vdW's contacts with the amino thiazole of dasatinib that are absent in the other complexes. The p-loop in BTK and Abl packs closer to the core of the kinase as evidenced by the shorter distance between the methyl substituent of the pyrimidine ring and the p-loop of BTK (8.69 Å to Gly^{411}) and Abl (7.12 Å to Gly^{250}) in comparison to EphA4 (9.85 Å to Gly^{630}), thereby partially shielding dasatinib from solvent. The position of the p-loop may relate to the differences in affinity for dasatinib noted in Fig. 5A.

4. Conclusion

We have elucidated the structure of the native EphA4 kinase domain and the first structure of this domain in complex with an inhibitor. The structure of the native kinase domain suggests that the JMS in EphA4 is not responsible for the change in the relative position of the αC-helix as was previously suggested [16]. In addition, the structure reveals a hydrophobic back-pocket in the ATP-binding site of EphA4 which was unknown before. The crystal structure of EphA4 in complex with dasatinib revealed a binding mode closely related to the one exhibited by Src family members, c-Src and Lyn.

Access to the hydrophobic pocket is governed by the gatekeeper residue while the size of the pocket appears to be governed by the position of the Lys–Glu salt bridge. The gatekeeper residue is conserved among 12 of the 14 human Eph receptors while, in our structure, the position of the conserved salt bridge is shifted, offering a larger hydrophobic pocket than in the other Eph receptors. This unique combination of gatekeeper and position of the salt bridge suggests a manner to design new, EphA4 specific inhibitors. Further mutational experiments targeting the ATP binding site and the hydrophobic pocket in particular could shed light on the potential to develop EphA4 specific compounds.

5. PDB accession numbers

Atomic coordinate and structure factors of apo- EphA4 and dasatinib-EphA4 were deposited in the Protein Data Bank under accession numbers 2Y6M and 2Y6O, respectively.

Acknowledgements

We would like to thank beamline scientists at the ESRF and SLS synchrotron facilities for their assistance during data collection. We acknowledge the Dutch Technologiestichting STW for funding this project.

Appendix A. Supplementary data

Supplementary data associated with this article can be found, in the online version, at doi:10.1016/j.febslet.2011.10.028.

References

[1] van der Geer, P., Hunter, T. and Lindberg, R.A. (1994) Receptor protein-tyrosine kinases and their signal transduction pathways. Annu. Rev. Cell Biol. 10, 251–337.
[2] Cheng, N., Brantley, D.M. and Chen, J. (2002) The ephrins and Eph receptors in angiogenesis. Cytokine Growth Factor Rev. 13, 75–85.
[3] Pasquale, E.B. (2008) Eph-ephrin bidirectional signaling in physiology and disease. Cell 133, 38–52.
[4] (1997). Unified nomenclature for Eph family receptors and their ligands, the ephrins. Eph Nomenclature Committee. Cell 90, 403–404.
[5] Pasquale, E.B. (2005) Eph receptor signalling casts a wide net on cell behaviour. Nat. Rev. Mol. Cell Biol. 6, 462–475.
[6] Bergemann, A.D., Zhang, L., Chiang, M.K., Brambilla, R., Klein, R. and Flanagan, J.G. (1998) Ephrin-B3, a ligand for the receptor EphB3, expressed at the midline of the developing neural tube. Oncogene 16, 471–480.
[7] Gale, N.W. et al. (1996) Elk-L3, a novel transmembrane ligand for the Eph family of receptor tyrosine kinases, expressed in embryonic floor plate, roof plate and hindbrain segments. Oncogene 13, 1343–1352.
[8] Gale, N.W. et al. (1996) Eph receptors and Ligands comprise Two major Specificity subclasses and are reciprocally compartmentilized during embryogenesis. Neuron 17, 9–19.
[9] Gong, J. et al. (2010) Use of protein array to investigate receptor tyrosine kinases activated in gastric cancer. Int. J. Oncol. 36, 101–106.
[10] Ashida, S. et al. (2004) Molecular features of the transition from prostatic intraepithelial neoplasia (PIN) to prostate cancer: genome-wide gene-expression profiles of prostate cancers and PINs. Cancer Res. 64, 5963–5972.
[11] van Doorn, R., Dijkman, R., Vermeer, M.H., Out-Luiting, J.J., van der Raaij-Helmer, E.M., Willemze, R. and Tensen, C.P. (2004) Aberrant expression of the tyrosine kinase receptor EphA4 and the transcription factor twist in Sezary syndrome identified by gene expression analysis. Cancer Res. 64, 5578–5586.
[12] Goldshmit, Y., Galea, M.P., Wise, G., Bartlett, P.F. and Turnley, A.M. (2004) Axonal regeneration and lack of astrocytic gliosis in EphA4-deficient mice. J. Neurosci. 24, 10064–10073.
[13] Murai, K.K. and Pasquale, E.B. (2003) 'Eph'ective signaling: forward, reverse and crosstalk. J. Cell Sci. 116, 2823–2832.
[14] Binns, K.L., Taylor, P.P., Sicheri, F., Pawson, T. and Holland, S.J. (2000) Phosphorylation of tyrosine residues in the kinase domain and juxtamembrane region regulates the biological and catalytic activities of Eph receptors. Mol. Cell. Biol. 20, 4791–4805.
[15] Wybenga-Groot, L.E., Baskin, B., Ong, S.H., Tong, J., Pawson, T. and Sicheri, F. (2001) Structural basis for autoinhibition of the Ephb2 receptor tyrosine kinase by the unphosphorylated juxtamembrane region. Cell 106, 745–757.
[16] Wiesner, S., Wybenga-Groot, L.E., Warner, N., Lin, H., Pawson, T., Forman-Kay, J.D. and Sicheri, F. (2006) A change in conformational dynamics underlies the activation of Eph receptor tyrosine kinases. EMBO J. 25, 4686–4696.
[17] Shah, N.P., Tran, C., Lee, F.Y., Chen, P., Norris, D. and Sawyers, C.L. (2004) Overriding imatinib resistance with a novel ABL kinase inhibitor. Science 305, 399–401.
[18] Lombardo, L.J. et al. (2004) Discovery of *N*-(2-chloro-6-methyl- phenyl)-2-(6-(4-(2-hydroxyethyl)-piperazin-1-yl)-2-methylpyrimidin-4- ylamino)thiazole-5-carboxamide (BMS-354825), a dual Src/Abl kinase inhibitor with potent antitumor activity in preclinical assays. J. Med. Chem. 47, 6658–6661.
[19] Li, J. et al. (2010) A chemical and phosphoproteomic characterization of dasatinib action in lung cancer. Nat. Chem. Biol. 6, 291–299.
[20] Karaman, M.W. et al. (2008) A quantitative analysis of kinase inhibitor selectivity. Nat. Biotechnol. 26, 127–132.
[21] O'Hare, T. et al. (2005) In vitro activity of Bcr-Abl inhibitors AMN107 and BMS-354825 against clinically relevant imatinib-resistant Abl kinase domain mutants. Cancer Res. 65, 4500–4505.
[22] Kabsch, W. (2010) Xds. Acta Crystallogr. D Biol. Crystallogr. 66, 125–132.
[23] Evans, P. (2006) Scaling and assessment of data quality. Acta Crystallogr. D Biol. Crystallogr. 62, 72–82.
[24] Winn, M.J. et al. (2011) Overview of the current CCP4 suite and current developments. Acta Crystallogr. D. 67, 235–242.
[25] Navaza, J. (2001) Implementation of molecular replacement in AMoRe. Acta Crystallogr. D Biol. Crystallogr. 57, 1367–1372.
[26] Langer, G., Cohen, S.X., Lamzin, V.S. and Perrakis, A. (2008) Automated macromolecular model building for X-ray crystallography using ARP/wARP version 7. Nat. Protoc. 3, 1171–1179.
[27] Murshudov, G.N., Vagin, A.A. and Dodson, E.J. (1997) Refinement of macromolecular structures by the maximum-likelihood method. Acta Crystallogr. D Biol. Crystallogr. 53, 240–255.
[28] Adams, P.D. et al. (2010) PHENIX: a comprehensive Python-based system for macromolecular structure solution. Acta Crystallogr. D Biol. Crystallogr. 66, 213–221.
[29] Emsley, P. and Cowtan, K. (2004) Coot: model-building tools for molecular graphics. Acta Crystallogr. D Biol. Crystallogr. 60, 2126–2132.
[30] Kornev, A.P., Taylor, S.S. and Ten Eyck, L.F. (2008) A helix scaffold for the assembly of active protein kinases. Proc. Natl. Acad. Sci. USA 105, 14377–14382.
[31] Hubbard, S.R., Mohammadi, M. and Schlessinger, J. (1998) Autoregulatory mechanisms in protein-tyrosine kinases. J. Biol. Chem. 273, 11987–11990.
[32] Huse, M. and Kuriyan, J. (2002) The conformational plasticity of protein kinases. Cell 109, 275–282.
[33] Cowan-Jacob, S.W., Mobitz, H. and Fabbro, D. (2009) Structural biology contributions to tyrosine kinase drug discovery. Curr. Opin. Cell Biol. 21, 280–287.
[34] Nowakowski, J. et al. (2002) Structures of the cancer-related Aurora-A, FAK, and EphA2 protein kinases from nanovolume crystallography. Structure 10, 1659–1667.
[35] Kay, L.E., Muhandiram, D.R., Farrow, N.A., Aubin, Y. and Forman-Kay, J.D. (1996) Correlation between dynamics and high affinity binding in an SH2 domain interaction. Biochemistry 35, 361–368.
[36] Liu, Y., Shah, K., Yang, F., Witucki, L. and Shokat, K.M. (1998) A molecular gate which controls unnatural ATP analogue recognition by the tyrosine kinase v-Src. Bioorg. Med. Chem. 6, 1219–1226.
[37] Daub, H., Specht, K. and Ullrich, A. (2004) Strategies to overcome resistance to targeted protein kinase inhibitors. Nat. Rev. Drug. Discov. 3, 1001–1010.
[38] Getlik, M., Grutter, C., Simard, J.R., Kluter, S., Rabiller, M., Rode, H.B., Robubi, A. and Rauh, D. (2009) Hybrid compound design to overcome the gatekeeper T338M mutation in cSrc. J. Med. Chem. 52, 3915–3926.
[39] Williams, N.K., Lucet, I.S., Klinken, S.P., Ingley, E. and Rossjohn, J. (2009) Crystal structures of the Lyn protein tyrosine kinase domain in its Apo- and inhibitor-bound state. J. Biol. Chem. 284, 284–291.
[40] Tokarski, J.S. et al. (2006) The structure of Dasatinib (BMS-354825) bound to activated ABL kinase domain elucidates its inhibitory activity against imatinib-resistant ABL mutants. Cancer Res. 66, 5790–5797.
[41] Marcotte, D.J. et al. (2010) Structures of human Bruton's tyrosine kinase in active and inactive conformations suggest a mechanism of activation for TEC family kinases. Protein Sci. 19, 429–439.